ISSN 1063-7850, Technical Physics Letters, 2018, Vol. 44, No. 1, pp. 1–16. © Pleiades Publishing, Ltd., 2018.
Original Russian Text © S.A. Blokhin, N.A. Maleev, M.A. Bobrov, A.G. Kuzmenkov, A.V. Sakharov, V.M. Ustinov, 2018, published in Pis'ma v Zhurnal Tekhnicheskoi Fiziki, 2018, Vol. 44, No. 1, pp. 7–43.

High-Speed Semiconductor Vertical-Cavity Surface-Emitting Lasers for Optical Data-Transmission Systems (Review)

S. A. Blokhin[a]*, N. A. Maleev[a, b], M. A. Bobrov[a], A. G. Kuzmenkov[a, c], A. V. Sakharov[a], and V. M. Ustinov[a, c, d]

[a] *Ioffe Physical Technical Institute, St. Petersburg, 194021 Russia*

[b] *St. Petersburg State Electrotechnical University, St. Petersburg, 197022Russia*

[c] *Submicron Heterostructures for Microelectronics Research and Engineering Center, Russian Academy of Sciences, St. Petersburg, 194021 Russia*

[d] *Peter the Great St. Petersburg Polytechnic University, St. Petersburg, 195251 Russia*

**e-mail: blokh@mail.ioffe.ru*

Received September 27, 2017

Abstract—The main problems of providing a high-speed operation semiconductor lasers with a vertical microcavity (so-called "vertical-cavity surface-emitting lasers") under amplitude modulation and ways to solve them have been considered. The influence of the internal properties of the radiating active region and the electrical parasitic elements of the equivalent circuit of lasers are discussed. An overview of approaches that lead to an increase of the cutoff parasitic frequency, an increase of the differential gain of the active region, the possibility of the management of mode emission composition and the lifetime of photons in the optical microcavities, and reduction of the influence of thermal effects have been presented. The achieved level of modulation bandwidth of ~30 GHz is close to the maximum achievable for the classical scheme of the direct-current modulation, which makes it necessary to use a multilevel modulation format to further increase the information capacity of optical channels constructed on the basis of vertical-cavity surface-emitting lasers.

DOI: 10.1134/S1063785018010054

1. INTRODUCTION

Recent years have seen active introduction of high-speed (10–25 Gbit/s) optical data-transmission channels with relatively small lengths (150 m) in data centers and supercomputers. A wide use of multimode optical fibers and surface-emitting semiconductor lasers with vertical microcavities (so-called "vertical-cavity surface-emitting lasers" (VCSELs)) in the near-IR range is typical for these applications. The key advantages of VCSELs over semiconductor lasers of classical design with output of emission through the end faces of a Fabry–Pérot resonator are a high-speed operation in the mode of direct-current modulation, a narrow symmetric diagram of the output emission, increased temperature stability of the output power and generation wavelength, group technology of manufacture, and the possibility of testing devices on a substrate prior to its separation into individual laser crystals [1].

The idea of vertical-cavity surface-emitting lasers was proposed in the late 1970s [2], but remarkable progress and the implementation of lasers that are suitable for practical use become possible only at the end of the 1990s, with the development of modern methods for epitaxial synthesis of complex multilayer heterostructures [3]. A high-speed operation under direct-current modulation is one of the key advantages of VCSELs, since this method of modulation is much easier in terms of technical implementation than are high-speed transmitters based on lasers with distributed feedback (DFB lasers) and high-speed integrated modulators. In comparison with lasers with Fabry–Pérot and a diagram of direct-current modulation, in this case, VCSELs provide a higher range of the limit of the modulation frequencies with better stability of characteristics and lower power consumption.

The amplitude-shift keying of the intensity of the optical carrier (i.e., laser emission) using a linear two-level code without a return to the level of the logical zero—NRZ (nonreturn to zero)—is widely used in ultrafast optical data-transmission channels based on VCSELs. The first reports of overcoming of the threshold of the data-transfer rate of 10 Gbit/s in the amplitude-modulation mode appeared in 2001, with IBM researchers obtaining a speed of 20 Gbit/s using

a VCSEL based on GaAs quantum wells with a spectral range of 850 nm and an oxide current-aperture of 8 μm as an active element in an optical transmitter [4]. The next increase in performance occurred in 2006, when NEC researchers showed that a data-transfer rate of 25 Gbit/s can be achieved using a VCSEL on the basis of InGaAs quantum wells with a spectral range of 1100 nm and an current-oxide aperture of 7 μm [5]. A year later, researchers from the same company reported the implementation of a 30-Gbit/s data-transmission optical line on the basis of a VCSEL with the spectral range of 1100 nm with a buried-tunnel junction [6]. Six months later, researchers from the University of California set a new record, demonstrating optical data transmission via an optical fiber at a speed of 35 Gbit/s using a VCSEL on the basis of InGaAs quantum wells with a spectral range of 980 nm and an current-oxide aperture of 3 μm [7]. Literally three months later, NEC researchers set a new record for the data-transmission rate in the direct modulation mode—40 Gbit/s—using a VCSEL on the basis of InGaAs quantum wells with a spectral range of 1100 nm and a current aperture of 6 μm [8]. It took considerably more time to overcome the milestone of 35 Gbit/s in the case of VCSELs with a spectral range of 850 nm: in 2008, the rate of 25 Gbit/s per channel using a VCSEL on the basis of InGaAs quantum wells with an current-oxide aperture of 9 μm was first achieved [9], and then a rate of 30 Gbit/s was attained for VCSELs on the basis of GaAs quantum wells with an current-oxide aperture of 6 μm [10]. In 2009, data-transfer rates of 32 [11] and 38 Gbit/s [12] for VCSELs on the basis of InGaAs quantum wells with a spectral range of 850 nm with an current-oxide aperture of 9 μm were consecutively demonstrated. Finally, the milestone of 40 Gbit/s was overcome in 2011 using a VCSEL on the basis of InGaAs quantum wells with a spectral range of 850 nm and an current-oxide aperture of 7 μm [13]. In the same year, a new data-transmission-rate record of 44 Gbit/s was set with the use of a VCSEL on the basis of InGaAs quantum wells with a spectral range of 980 nm and an current-oxide aperture of 6 μm [14]. However, this record was already broken in 2013: data-transmission rates of 47 [15] and 57 Gbit/s [16] were shown for VCSELs on the basis of InGaAs quantum wells with a spectral range of 850 nm and a current-oxide aperture of 7–8 μm. At present, the data-transmission rate of 57 Gbit/s per channel is the absolute record for direct modulation of VCSELs of the near-infrared range with the use of the classical NRZ code.

The main problems of providing a high-speed operation of a VCSEL during amplitude modulation and ways to solve them are considered in this review.

2. VCSEL PERFORMANCE UNDER DIRECT MODULATION

When a VCSEL is used in high-speed optical systems for data transmission, a digital optical signal generated by direct-current modulation should be transmitted into the active area for electro-optical conversion without significant losses or distortions. The frequency characteristics for any injection laser in the mode of direct-current modulation are determined by both the internal properties of its radiating active region (a so-called "ideal laser") and electrical parasitic elements of the equivalent circuit of the device (the capacitance, resistance, and inductance), which form a low-pass *RC* filter. The parasitic elements can be isolated from the ideal laser by determining the directly light-emitting region, in which charge carriers and photons interact via the processes of absorption, spontaneous emission, and stimulated emission, as the last one within the equivalent four-terminal network model [17]. The structure of the *RC* filter includes external parasitic elements connected with contact pads, as well as internal parasitic elements, which are associated with the regions of laser structure between the metal contacts and the light-emitting area, which, in the case of a VCSEL, is limited in the lateral direction of the current aperture. In such a context, the dynamic model of the ideal laser is based on the systems of phenomenological velocity equations [18], while the frequency properties of the *RC* filter are determined by the parameters of the parasitic elements of the equivalent electric circuit of the device.

The frequency response of a semiconductor laser—the amplitude–frequency characteristic (AFC)—is determined by multiplying transfer function f of a low-pass filter of the second order with a damping factor (the transfer function of an ideal laser) and functions $H_{\text{int}}(f)$ of the low-pass filter of the first order (the transfer function of the *RC* filter) during harmonic modulation of the pumping current with frequency I_0 for a given constant operating current $H_{\text{int}}(f)$ that defines the so-called "current operating point" [18]:

$$H(f) = \text{const}\left[\frac{f_R^2}{f_R^2 - f^2 + j\gamma(f/2\pi)}\right]\left[\frac{1}{1 + j(f/f_p)}\right], \quad (1)$$

where f_R is the resonance frequency, γ is the damping factor of the relaxation oscillations, and f_p is the parasitic cutoff frequency. Frequency of the relaxation oscillations of the ideal laser f_r, which characterizes the dynamics of the interaction between the injected charge carriers and generated photons, can be written as

$$f_R = \frac{1}{2\pi}\left[\frac{N_p V_g}{\tau_p}\frac{g_N}{\chi}\right]^{1/2} = \frac{1}{2\pi}\left[\frac{v_g \eta_i}{qV_p}\frac{g_N}{\chi}\right]^{1/2}\sqrt{I_0 - I_{th}} = D\sqrt{I_0 - I_{th}}, \quad (2)$$

where N_p is the density of photons in the laser cavity; τ_p is the lifetime of photons in the cavity; g_N is the differential gain of the active region of the laser; v_g is the group velocity of photons; $\chi = 1 + \tau_s/\tau_e$ is the transport coefficient, which takes into account time of carrier transportation to the active region through the undoped part of the cavity τ_s and characteristic time of the thermal carrier emission from the active region τ_e; η_i is the internal quantum efficiency; V_p is the volume of the considered optical mode of the cavity; q is the elementary charge; and I_{th} is the threshold current of the laser. The rate of the increase of the relaxation frequency with current (the so-called "D factor") determines how fast the ideal laser can be modulated. However, the notion of effective laser modulation of frequency $f_{-3\text{dB}}$ by the level of AFC decay of –3 dB (the so-called "modulation bandwidth") at a given operating current and a current-modulation efficiency (the so-called "MCEF factor"), which are associated by relation (3), are used to describe the real laser-frequency response:

$$f_{-3\text{dB}} = \text{MCEF}\sqrt{I_0 - I_{th}}. \quad (3)$$

It should be noted that the maximum data-transfer rate F in the direct modulation mode is connected with the modulation bandwidth frequency of the laser by the empirical relation [19]

$$F \sim 1.55 f_{-3\text{dB}}. \quad (4)$$

In the general case, the achievable laser-modulation bandwidth is limited by three mechanisms: thermal effects, damping of the relaxation oscillations, and the parasitic cutoff frequency of the *RC* filter, each of which has its own theoretical limit for the maximum modulation bandwidth when the influence of other mechanisms is neglected.

According to expression (2), the most direct way to increase modulation bandwidth of the VCSEL is by increasing the photon density in the cavity through means of increasing the pumping current. However, the self-heating of the laser with increasing current leads to a decrease in the population inversion and reduction of the gain of the active region. As a result, the maximum achievable modulation bandwidth, which is limited by thermal effects, is determined by the expression

$$f_{-3\text{dB,thermal}} \approx \sqrt{1+\sqrt{2}} f_{R,\max}. \quad (5)$$

Note that this effect is also accompanied by a further increase in the damping factor of the relaxation oscillations due to the growing contribution of the gain nonlinearity to the K factor. Not only must the thermal resistance and power-dissipation level be reduced to increase the laser-modulation bandwidth, but the differential gain of the active region must be increased and the mode volume reduced.

The damping rate of the relaxation oscillations increases quadratically with the growth of the resonance frequency:

$$\gamma = K f_R^2 + \gamma_0, \quad (6)$$

$$K = 4\pi^2(\tau_p + \tau_g) = 4\pi^2\left(\frac{L_c}{v_g(A_{\text{int}} + T_m)} + \frac{\varepsilon\chi}{g_N}\right), \quad (7)$$

where τ_p is the lifetime of photons in the cavity, τ_g is the component that is responsible for the nonlinearity of the gain, A_{int} is the internal loss, T_m is the mirror loss, L_c is the effective length of the microcavity, ε is the coefficient of gain nonlinearity that describes the drop in the gain of the active region with the increase of the concentration of photons (the so-called "gain compression"), and γ_0 is the offset due to the contribution of the spontaneous emission into the laser mode. The maximum achievable modulation bandwidth, which is limited by the damping of the relaxation oscillations, is determined by expression (8) in the case of a dominant influence of the effect of the damping of the relaxation oscillations at a high density of photons (when it is possible to neglect the contribution of the spontaneous emission to the laser mode):

$$f_{-3\text{dB,damping}} = \sqrt{2}\frac{2\pi}{K}. \quad (8)$$

It follows from relations (6)–(8) that the lifetime of photons in the resonator should be reduced, the differential gain of the active region should be increased, and the coefficient of gain nonlinearity should be reduced to improve the laser-modulation bandwidth.

In a real laser, the parasitic capacitance and resistance form a low-pass *RC* filter, which shunts the modulating current parallel to the active region at frequencies that exceed the bandwidth of the *RC* filter. In the case of a dominant influence of the *RC* filter, the maximum achievable modulation bandwidth is determined by the expression

$$f_{-3\text{dB,parasitics}} = (2+\sqrt{3}) f_p. \quad (9)$$

It is clear that improvement of the performance of a laser is associated with a decrease in the parasitic capacitance and resistance of the device.

As a result, in practice, a complex system of related tasks has to be solved:

—increasing the differential gain of the active medium;

—reducing the coefficient of gain nonlinearity;

—reducing the lifetime of photons;

—increasing the density of photons in the resonator;

—reducing the mode volume;

—reducing the thermal resistance of the laser; and

—increasing the parasitic frequency of the *RC* filter.

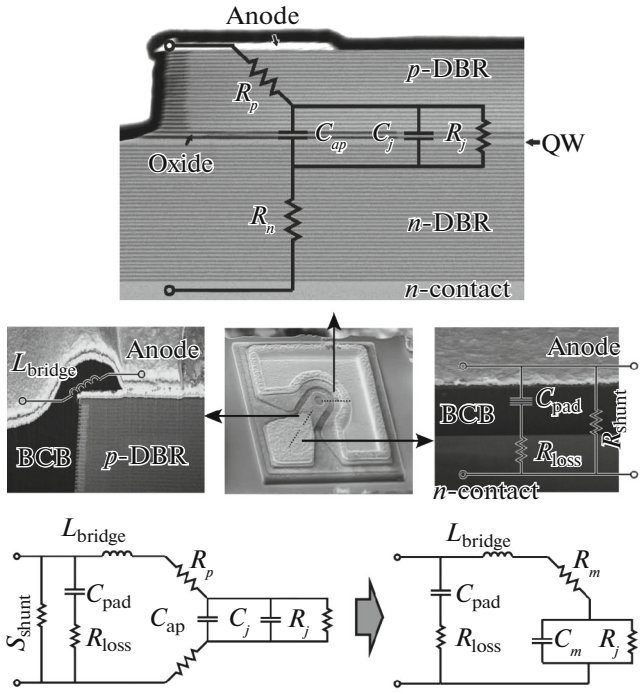

Fig. 1. The equivalent circuit of a VCSEL with conductive DBRs and a selectively oxide-current aperture. DBR, distributed Bragg reflector; QW, quantum well. $R_m = R_p + R_n$, $C_m = C_{ap} + C_j$.

3. INCREASING THE PARASITIC CUTOFF FREQUENCY

The following main components can be distinguished in the equivalent circuit of a VCSEL in a general case (Fig. 1): resistance R_{shunt} (usually a negligibly small value), which is responsible for leakage currents, which are determined by the insulating properties of the material under the contact pads and condition of the surface between the contacts; capacitance C_{pad}, which depends on the topology of the contact pads and characteristics of the used dielectrics; resistance R_{loss}, which takes into account the losses in the current flow through the contact pads at high frequency; inductance L_{bridge}, which is formed between the contact substrate and metallization of the laser of one type of conductivity; resistances R_n and R_p, which correspond to doped mirrors or intracavity contacts of an appropriate conductivity type when a current flows through them; capacitance C_{ap}, which is formed on the oxide layers of AlGaO; resistance R_j, which describes the resistance of the p–n junction of the ideal laser; capacitance C_j, which is formed by a directly shifted p–n junction of the ideal laser in the area of the current aperture. Usually, inductance L_{bridge} is small, and so such an equivalent circuit of the laser corresponds to a circuit of two cascaded low-pass filters of the first order. However, in practice, the contribution of only one cascade with a lower cutoff frequency is vital, and, therefore, the *RC* filter of the first order is considered, as a rule, when VCSEL properties are being modeled. Thus, the increase in the parasitic cutoff frequency is due to the minimizing of the values of the main parasitic components of the equivalent circuit of the VCSEL. Herewith, the capacitances of the contact pads and ideal laser make the greatest contribution to the limiting of the modulation bandwidth.

A number of approaches have been proposed to minimize capacitance of the contact pads C_{pad}: minimization of the square of the signal contact pads [20], growing of the VCSEL heterostructure on undoped substrates [21], the removal of conductive layers under contact pads [22], and the use of insulating materials with low dielectric permeability under contact pads [7]. According to [23], the use of benzocyclobutene (BCB) or polyimide as an insulating material can reduce the capacitance of the contact pads to the level of a few tens of fF, while maintaining relatively low values of resistance R_{loss}. As a result, the cutoff frequency of the low-pass filter that is formed by the capacitances and resistances of the contact pads may be increased up to several tens of gigahertz, while the second low-pass filter, which is formed by capacitances and resistances of the inner regions of laser structure, will make the main contribution to the limitation of the modulation bandwidth.

A characteristic feature of VCSELs is a large number of heteroboundaries in the path of the injection of charge carriers into the active area. The presence of potential barriers at heteroboundaries (the most critical for holes) leads to a higher operating voltage and VCSEL series resistance, which ultimately leads to self-heating of the laser and a drop in the parasitic cutoff frequency. Various schemes of the modification of the band diagram of heteroboundaries in combination with the optimization of doping profiles have been proposed to reduce the series resistance of the laser (resistances R_n and R_p in the equivalent circuit) while maintaining a low level of optical losses: a step change in composition [24, 25], parabolic profiles of a composition change [26], and uniparabolic profiles of a change in the composition [27]. The "digital" gradients (digital alloy grading), which allow the formation of any effective profile of the composition change, are widely used in the case of epitaxial growing of VCSEL heterostructures using molecular-beam epitaxy [28, 29].

According to [30], the reduction of the thickness of the undoped part of a laser cavity leads to a decrease in p–n-junction capacitance C_j. However, the doping profile of the layers must take into account the distribution of the electromagnetic field of the standing wave in an optical microcavity to prevent additional optical losses at free carriers and the design of the

active region and its location relative to the profile of the electromagnetic field of the standing wave should provide a high modal gain. In this regard, the only effective way to reduce capacitance C_j is the decreasing of the current aperture area and operating currents, which is not always possible.

Relatively thin selectively oxidized current apertures are usually formed to suppress the effect of light scattering at the oxide–semiconductor boundary [31]. However, this is associated with high values of capacitance C_{ap}. Decreasing the area under the oxide layer by reducing the size of the laser mesa solves the problem only partially, because in practice the minimum diameter of the VCSEL mesa with the doped mirrors is limited to a size of the order of 20 μm, and even larger mesas are required for a VCSEL with intracavity contacts. In [32, 33], it was shown that an increase in the thickness of the oxide aperture leads to a proportional reduction of capacitance C_{ap} and the increasing of the parasitic cutoff frequency. The application of multilayer oxide structures to increase the thickness of the oxide effectively, while maintaining low values of resistances R_n and R_p, seems to be a logical development of the proposed approach due to the effect of the depletion of the doped layers in the vicinity of the oxide [34], [35]. The application of two quarter-wave oxide apertures reduces capacitance C_{ap} by 50% and allows the cutoff frequency to be increased up to 18 GHz [36], and the use of four additional oxide layers (with a smaller length in comparison with an current-oxide aperture) makes it possible to reduce the capacitance by another 30–40% and increase the cutoff frequency to 22 GHz [37].

An alternative approach to decreasing capacity C_{ap} is the use of proton implantation to increase the effective thickness of the nonconductive region above the aperture, which can reduce total laser capacitance $C_m = C_{ap} + C_j$ by three times and increase the cutoff frequency from 19 to 36 GHz [38]. However, despite a number of interesting results, this approach has not found wide practical application in the creation of a modulation bandwidth VCSEL [39].

4. DIFFERENTIAL GAIN OF THE ACTIVE REGION

The choice of a design for an active region is due to a greater extent to the requirements for laser-emission wavelength and the properties of the used materials. However, from the point of view of improving VCSEL frequency response, preference should be given to the design of the active region, which will provide the largest differential gain, which in turn will increase the resonance frequency without a significant increase in the operating current.

The most promising approach to increasing differential gain is the reduction in the density of the states in the active region that need to be filled by the charge carriers to obtain laser generation. According to [40], the differential gain of quantum wells (QWs) of GaAs in the spectral range of 850 nm (compared to InGaAs QWs with a spectral range of 980 nm) is limited by the high density of states in the valence band. In [41], it was theoretically shown that the differential amplification of highly strained quantum wells is three to four times higher than the differential gain of the lattice-matched quantum wells, which was later experimentally confirmed in works [42, 43]. An increase in the internal mechanical stresses (due to the increase in the In concentration) in a quantum well leads to the expulsion of a subband of light holes to the interior of the valence band and a shift of the Fermi quasi-level for holes to the edge of the band, providing a higher differential gain for the highly strained InGaAs quantum wells. The described approach showed its effectiveness during the implementation of a VCSEL that was based on highly strained InGaAs/GaAs quantum wells in the spectral range of 950–1100 nm and allowed the overcoming the data-transfer rate of 25 Gbit/s to be exceeded [5, 7, 44]. Recently, this concept has been successfully applied to a VCSEL with a spectral band of 850 nm [9]. According to the calculations described in [45], the addition of a small amount of In into a GaAs QW leads to an increase in the curvature of the valence band and splitting of the zones for heavy and light holes, which, together with the reduced thickness of the quantum well, reduces the density of states in the valence band and provides a twofold increase of differential gain. It should be noted that the density of states in the valence band of a strained InGaAs quantum well almost ceases to change when the In content achieves ~10%. In [46], it was shown that the use of $In_{0.07}Ga_{0.93}As$/AlGaAs quantum wells allows the modulation bandwidth of the VCSEL with a spectral range of 850 nm to be increased from 16.5 to 20 GHz. However, the low (~10 GHz) parasitic cutoff frequency of the implemented devices limited the rate of error-free modulation of data to a level of 32 Gbit/s [10].

It was suggested to use the approach described above in conjunction with the methods of reducing parasitic capacitance of the aperture C_{ap} to further increase the modulation bandwidth in the large signal mode. The calculated intensity distribution of the electromagnetic field and the refractive-index profile in the structure of this type of VCSEL with a spectral range of 850 nm with an active region based on InGaAs QWs are shown in Fig. 2. The design used a classical vertical microcavity with the upward output emission consisting of a concealed contact layer of n^+ type, a lower distributed Bragg reflector

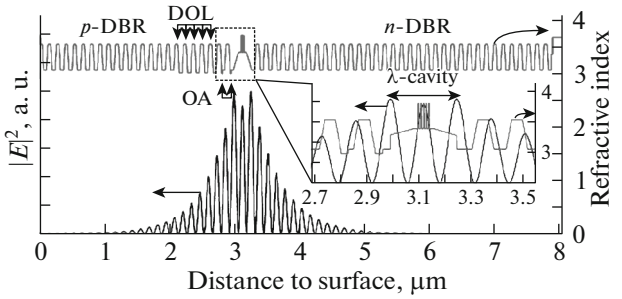

Fig. 2. The calculated electromagnetic-field distribution of the standing wave and the refractive-index profile in the structure of VCSEL with a spectral range of 850 nm with an active region on the basis of InGaAs QWs. Inset, the enlarged image of the central region of the optical microcavity. OA, aperture layers; DOL, additional layers with a smaller depth of oxidation in comparison with an oxide aperture; DBR, distributed Bragg reflector.

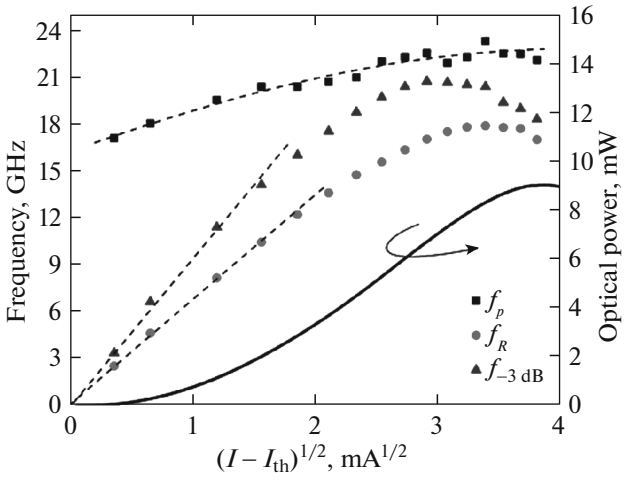

Fig. 3. Dependences of resonance frequency f_R, modulation bandwidth f_{-3dB}, parasitic cutoff frequency f_p, and output optical power on $\sqrt{I - I_{th}}$ for a VCSEL on the basis of InGaAs QWs with a spectral range of 850 nm with an oxide-current aperture of 9 μm. The temperature of measurements was 20°C.

(DBR) of *n* type $Al_{0.15}Ga_{0.85}As/Al_{0.9}Ga_{0.1}As$, a 1λ-AlGaAs microcavity with an active region, an upper DBR of *p* type $Al_{0.15}Ga_{0.85}As/Al_{0.9}Ga_{0.1}As$, and a surface contact layer of GaAs of p^+ type. The design of the optical microcavity with a separate restriction of carriers and a gradient profile of the composition change was used to provide fast capture of carriers into quantum wells and their effective localization. Several details should be taken into account when choosing the design of the active region on the basis of InGaAs QWs. On the one hand, the use of deeper quantum wells (with a high content of In) makes it necessary to reduce their thickness to retain the desired wavelength of active-region emission while simultaneously increasing the total number of wells and reducing the thickness of barrier layers between them to provide a high longitudinal factor of optical confinement and the desired modal gain [46]. On the other hand, it is necessary to take into account that the reduction of the thickness of the barrier layers between the quantum wells is associated not only with the probability of the formation of bounded states, but also with the possible formation of growth defects due to the accumulation of structural stresses. In this case, the active region contains five InGaAs QWs with an In content of 7–8% and a thickness of 4 nm, which are surrounded by barrier layers of $Al_{0.37}Ga_{0.63}As$ with a thickness of 6 nm. There are two aperture layers AlGaAs of *p* type with a stepped profile of the composition for Al, which are used to form the optical and current constraints in the lateral direction by the selective oxidation method in the vicinity of the microcavity from the side of the DBR of *p* type. Along with the use of a double oxide aperture, additional selectively oxidized AlGaAs layers, which were located in the DBR of *p* type and had a shallower depth of oxidation in comparison with the aperture layers (deep oxidation layer), were used to reduce the C_{ap} capacity.

The results of small-signal frequency analysis of such a VCSEL with a spectral range of 850 nm with an active region on the basis of InGaAs QWs and a double-current-oxide aperture with a size of 9 μm are presented in Fig. 3. It follows from the presented data that the modulation bandwidth exceeds the resonance frequency in the entire range of the operating currents, i.e., that the effect of damping of the relaxation oscillations is weak. Moreover, the parasitic cutoff frequency of the investigated lasers is in the range of 18–23 GHz and does not have a significant impact on their high-frequency properties according to the modeling of the frequency dependences of the reflection coefficient for the modulating microwave signal. The approach that was used to solve the problem of the parasitic *RC* filter improved the efficiency of the laser modulation by a microwave signal and implemented error-free data transfer at a speed of 38 Gbit/s [12].

According to theoretical studies [47, 48], the effective reduction of the density of states and the changing of the position of the Fermi level for holes can be achieved by the modulated doping of the active region by the acceptor impurity. However, experiments showed that, despite a significant (~50%) fall of the nonlinearity gain coefficient, there is only a relatively weak (15%) increase in the differential gain of the active region of the strained InGaAs quantum wells [43]. The published experimental data do not allow an unambiguous conclusion to be drawn regarding the

effect of doping on the differential gain of the active region in the case of lattice-matched GaAs quantum wells [49, 50]. It should be borne in mind that the accompanying increase in the internal optical losses due to the absorption on free carriers in conditions of a low level of modal gain of the active region, which is characteristic of lasers with vertical microcavities, limits greatly the effectiveness of this approach for VCSELs. At the present time, only investigation of the influence of δ doping of strained InGaAs/GaAs quantum wells on the speed response of the VCSEL with a spectral range of 1060 nm [51] can be distinguished, where the possibility of the increasing of the maximum bandwidth from 16.5 to 18.5 GHz by reducing the gain compression by approximately three times and the K factor by ~50% was shown and an error-free data transmission at a rate of up to 25 Gbit/s was demonstrated. At the same time, the doping of the active region with impurities of p type allows an efficient increase in the temperature stability of the dynamic characteristics of the VCSEL [52].

The modification of the kinetics of the emitting recombination of the active region is an alternative method of the increasing of the differential gain. According to theoretical calculations, the so-called "exciton mechanism" of recombination of carriers, leading in particular to a significant (up to twofold) increase of the differential gain, dominates in a semiconductor with centers of localization (e.g., quantum dots) [53]. Despite notable successes in the improving of the modulation bandwidth of end lasers on the basis of classical quantum dots grown in the Stranski–Krastanov growth mode [54], the implementation of effective high-speed VCSELs on the basis of quantum dots is limited by such problems as low material gain, which is due to the small surface density of dots [55], and a strong damping of the relaxation oscillations due to a pronounced effect of gain compression [56]. According to theoretical calculations [57], increasing the density of quantum dots to 10^{11} cm^{-2} and application of the vertical allocation technology for series of quantum dots (15–20 rows) potentially allow achieving a VCSEL bandwidth of ~10 GHz. In practice, however, the bandwidth of VCSELs based on InAs/InGaAs quantum dots with a spectral range of 1300 nm is limited to a bandwidth of ~2.5 GHz [58, 59].

The gain saturation and the drop of the differential gain of Stranski–Krastanov quantum dots are mainly related to their strong inhomogeneous broadening [60] and the completion of the wetting layer states by carriers [61], whereas the application of submonolayer InGaAs points or submonolayer InAs insertions in a GaAs quantum well potentially allows these drawbacks to be partially overcome while maintaining the exciton mechanism of recombination and suppression of the lateral transport of carriers [62]. Thus, in work [63], the possibility of operation of s VCSEL with a spectral range of 980 nm on the basis of submonolayer InGaAs quantum dots at s data-transfer rate of 20 Gbit/s and s laser temperature of up to 120° without changing the parameters of direct modulation was demonstrated. However, the use of highly strained InGaAs/GaAsP quantum wells with a spectral range of 980 nm allows better results to be achieved [64]. At the same time, the use of submonolayer InAs insertions as the active region of a VCSEL with a spectral range of 850 nm did not show notable advantages in comparison with GaAs quantum wells [65].

In contrast to classic Fabry–Pérot front-end lasers, in the case of VCSELs, it is necessary to coordinate spectrally the position of the maximum of the spectrum of the active region gain and the resonant wavelength of microcavity at a desired operating temperature not only to enhance the temperature stability of the threshold current and output power, but also to improve the dynamic characteristics of the device [18]. The resonance wavelength shift into a longer-wave region in comparison with the maximum of the spectrum of the active-region gain (so-called "negative detuning") can provide a higher differential gain at the wavelength of VCSEL generation and increase the bandwidth at an increased temperature [64, 66].

5. MANAGEMENT OF THE MODE COMPOSITION OF EMISSION

After solving the problem of low parasitic cutoff frequency, the most obvious way to increase the VCSEL resonance frequency is to increase the photon density in the cavity (see Eq. (2)). However, increasing of the photon density in the cavity by the raising of the concentration of the injected carriers (the density of the pumping current) leads to a significant growth (proportional to the third degree) of the degradation rate of the device [34, 67]. It should be taken into account that, in the case of the multimode VCSEL generation mode, it is necessary to consider separately the density of photons per every optical mode of the laser microcavity. For this reason, the growth rate of the resonance frequency, which is caused by the current increasing (the D factor), will be slower for a multimode laser than in the case of a single-mode laser [68]. Moreover, the competition for carriers between the individual modes can lead to a nonclassical type (more than one resonance) of frequency response of multimode lasers [69, 70].

The results of weak-signal frequency analysis of a VCSEL with a spectral range of 850 nm with an active region that is based on InGaAs QWs, which is implemented in the design in Fig. 2, are presented in Fig. 4. The main parameters that characterize the high-frequency properties of devices were constructed depending on the current-oxide-aperture size. The reducing of the size of the current-oxide aperture not

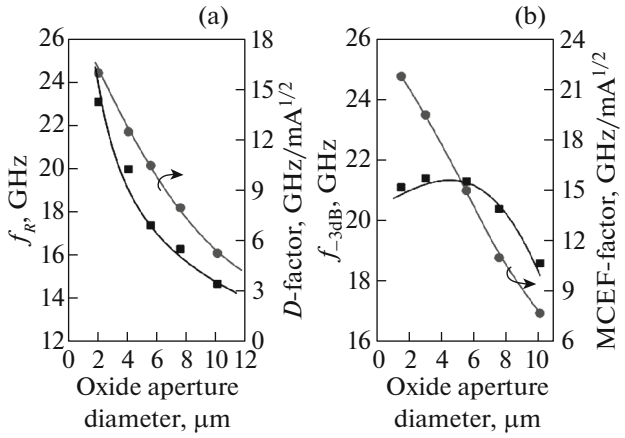

Fig. 4. VCSEL on the basis of InGaAs QWs with a spectral range of 850 nm. (a) Dependences of maximum resonance frequency f_R and the D factor on the size of the oxide-current aperture; (b) the dependences of maximum modulation bandwidth f_{-3dB} and the MCEF factor on the size of the oxide-current aperture. The temperature of measurements was 20°C.

only decreases the number of modes in the spectrum of the laser generation, but also reduces the modal volume, which leads to a substantial increase in the photon density for the potentially supported modes. As a result, the D factor increases with the decrease in the current aperture size (in the first approximation inversely proportional to the size) [71, 72]. This allows achieving higher resonant frequencies (Fig. 4a). However, a sharp increase in electrical and thermal resistances at a decrease in the lateral size of the current aperture leads to a strong self-heating of the lasers, which, in combination with the high values of the damping rate of relaxation oscillations, limits the range of the operating currents at which a high modulation bandwidth is achieved and limits the data-transmission rate for single-mode lasers to a level of 25 Gbit/s [73, 74]. As a result, the optimum size of the current aperture that provides a maximum the VCSEL modulation bandwidth typically lies in the range of 4–8 μm (Fig. 4b). At the same time, lasers with a current aperture of 3—4 μm, in which the factor of the suppression of higher-order modes (SMSRs) does not exceed 10–20 dB (so-called "quasi-single-mode lasers"), allow not only achieving high modulation bandwidth at low pumping currents, but also the reduction in the laser-generation spectrum width as compared to that for typical multimode VCSELs [32]. This approach is widely used to improve the energy efficiency of optical transmitters that are based on VCSELs and the range of data transmission along standard multimode fibers [75–77].

An alternative approach to increasing the photon density per laser consists in control of mode composition (decrease in the number of modes) in an initially multimode wide-aperture device by the incorporating of selective optical losses and/or an additional optical confinement. For example, the formation of the optical aperture with a high level of absorption on free carriers using the zinc local-diffusion technology allows increasing the power of single-mode emission of the VCSEL with a spectral range of 850 nm with an active region that is based on GaAs QWs and a current-oxide aperture. However, despite the growth of the D factor, the resonance frequency for such devices quickly becomes saturated with increasing current due to spatial "hole burning" in the gain spectrum, which ultimately limits the modulation bandwidth to a level of 12 GHz [78]. Optical-aperture creation by the creation of a spatially ordered array of etched holes in the output mirror of the VCSEL with a spectral range of 850 nm with an active region that is based on GaAs QWs and a current aperture that is obtained by ion implantation allows the creation of single-mode lasers with a modulation bandwidth of more than 18 GHz and an error-free data-transmission rate of 25 Gbit/s [79]. However, the low output optical power and relatively high threshold current [80], together with the technological complexity of creating such an optical aperture, limit the practical use of this approach. The creation of surface relief by local etching of the output mirror to a depth that is a multiple of the thickness of a quarter-wave DBR layer is the most promising way to control the VCSEL-mode composition [81]. However, this approach is not useful for providing a significant increase in the VCSEL modulation bandwidth [82] and is primarily used to increase the data-transmission range while maintaining an acceptably high rate [83, 84].

6. MANAGING THE LIFETIME OF PHOTONS IN A CAVITY

According to expression (6), the increase of resonance frequency f_R leads at the same time to a higher damping rate of the relaxation oscillations. It is necessary to reduce the K factor to increase modulation bandwidth f_{-3dB} with growth of the resonance frequency. Unfortunately, effective methods to control nonlinearity coefficient of the active-region gain ε have yet to be proposed and an increase in differential gain of the active region g_N, which provides an increase in resonance frequency f_R, can simultaneously lead to a significant increase in gain compression [51]. The most promising approach to mitigating the effect of the damping of the relaxation oscillations is connected with a decrease in lifetime of photons in the cavity τ_p, which can be done by reducing the reflection coefficient of the output mirror by changing the number of pairs of quarter-wave layers in the DBR or changing the thickness of the near-surface layer of the DBR. As an example, the evolution of the watt and volt–ampere characteristics of the VCSEL with a spectral range of 850 nm based on InGaAs QWs with a current-oxide aperture of 5.5 μm in the design that is shown in

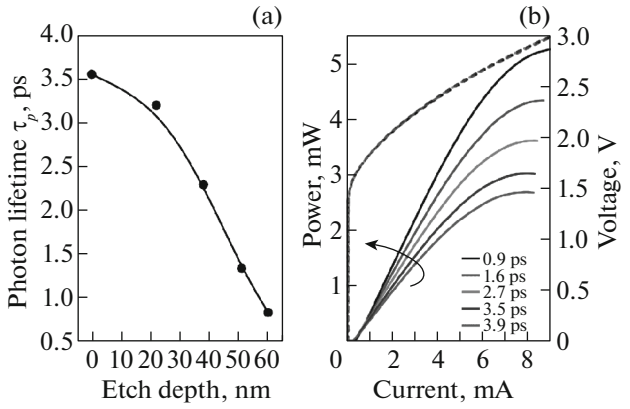

Fig. 5. VCSEL on the basis of InGaAs QWs with a spectral range of 850 nm with a current-aperture diameter of 5.5 μm. (a) The dependence of the lifetime of photons in the cavity on the depth of the etching of the near-surface layer of a DBR, (b) volt and watt–ampere characteristics of the laser at different lifetimes of photons in the cavity. The temperature of measurements was 20°C.

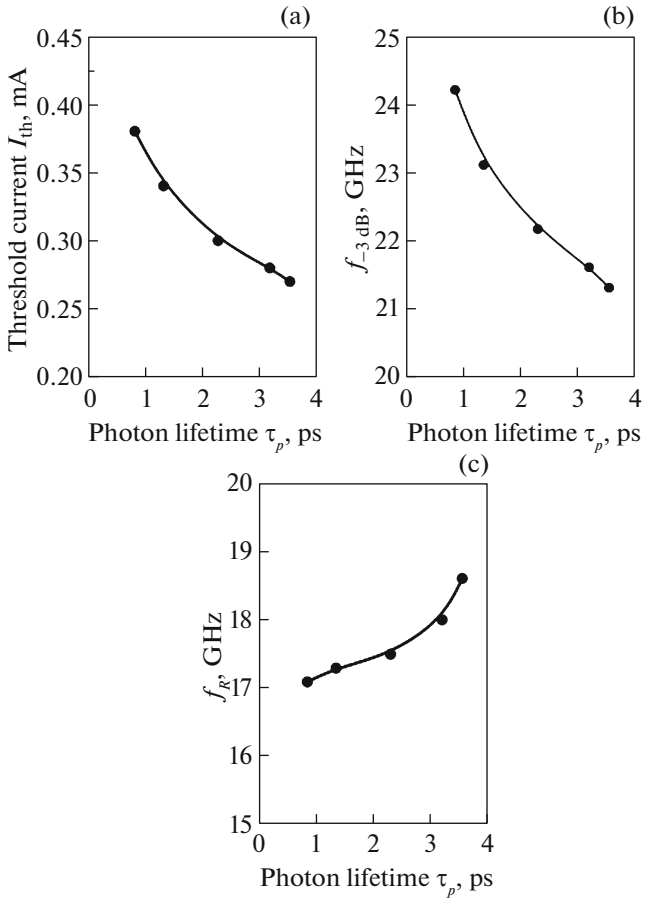

Fig. 6. VCSEL on the basis of InGaAs QWs with a spectral range of 850 nm with a current–aperture diameter of 5.5 μm. (a) The dependences of threshold current I_{th}, (b) the limit values of effective-modulation frequency f_{-3dB}, and (c) resonant frequency f_R on the lifetime of photons in the cavity. The temperature of measurements was 20°C.

Fig. 2 is presented in Fig. 5. The last version allows the controlling lifetime of photons in the cavity τ_p without a noticeable deterioration of the current-voltage characteristics of lasers and avoid an uncontrollable dispersion of the VCSEL characteristics, which is due to the heterogeneity of the laser epitaxial structure or an unevenness when performing postgrowth operations to modify the number of pairs of quarter-wave layers in the DBR. In [85], it was shown for the first time that the decrease in lifetime τ_p from 6.4 to 3.3 ps for the VCSEL with a spectral range of 850 nm with an active area on the basis of InGaAs quantum wells leads to a 50% drop in the K factor and a corresponding increase in modulation bandwidth f_{-3dB} from 15 to 23 GHz, which ultimately made it possible to achieve an error-free data-transmission rate of 40 Gbit/s in multimode VCSELs [86].

However, this approach has its limitations. On the one hand, the reduction of the lifetime of photons in the cavity allows increasing the maximum of the modulation bandwidth (Fig. 6b). On the other hand, reduction of the reflection coefficient of the output mirror is accompanied by an increased optical loss in output emission T_m and a corresponding increase of the threshold current (Fig. 6a), since a higher carrier density in the active region will be required to achieve the laser-generation conditions. In turn, an increase of the threshold current leads to a decrease in differential gain g_N, decrease of resonance frequency f_R (Fig. 6c), and, at maximum losses in output emission T_m and significant internal optical losses, to a decrease in maximum modulation bandwidth f_{-3dB}. As a result, there is an optimal lifetime of photons in the cavity τ_p, at which the highest modulation bandwidth f_{-3dB} is achieved, for each specific VCSEL design [13, 87]. It should be noted that the value of the optimal lifetime of photons in the cavity τ_p and magnitude of the change of the modulation bandwidth also depend on the current-aperture size [37].

The ratios of modulation bandwidth f_{-3dB} to resonance frequency f_R depending on the pumping current for the VCSEL with a spectral range of 850 nm on the basis of InGaAs QWs in the design that is shown in Fig. 2 are presented in Fig. 7a. It should be noted that the parasitic cutoff frequency of the considered devices is greater than 20 GHz and has no significant effect on frequency response of the investigated lasers. In wide-aperture lasers, the ratio of modulation bandwidth f_{-3dB} to resonant frequency f_R tends to the theoretical limit of 1.55, which corresponds to the case in which thermal effects are the limiting mechanism (Fig. 7a). At the same time, there is a sharp drop of ratio f_{-3dB}/f_R with an increasing in the pumping cur-

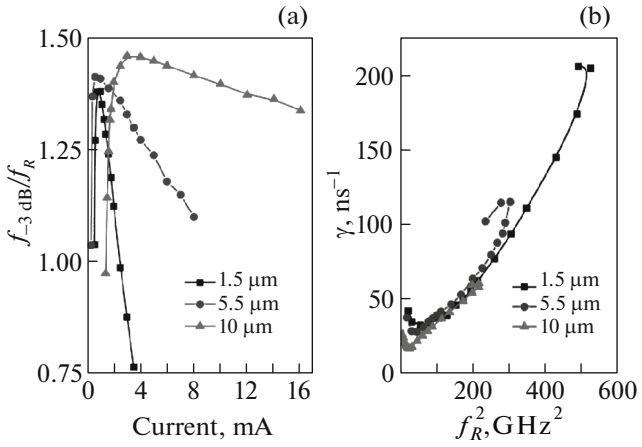

Fig. 7. VCSEL on the basis of InGaAs QWs with a spectral range of 850 nm with a current–aperture diameter of 1.5, 5.5, and 10 μm. (a) The dependences of the ratio of modulation bandwidth f_{-3dB} to resonance frequency f_R on the pumping current, (b) the dependences of the attenuation coefficient on the square of the resonance frequency. The temperature of measurements is 20°C.

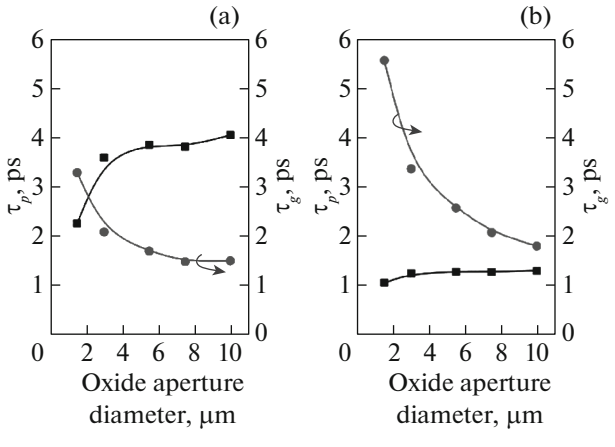

Fig. 8. The dependences of lifetime of photons in the cavity τ_p and nonlinearity gain τ_g on the size of the oxide-current aperture at (a) low and (b) high levels of losses per emission output for the VCSEL on the basis of InGaAs QWs with a spectral range of 850 nm. The temperature of measurements is 20°C.

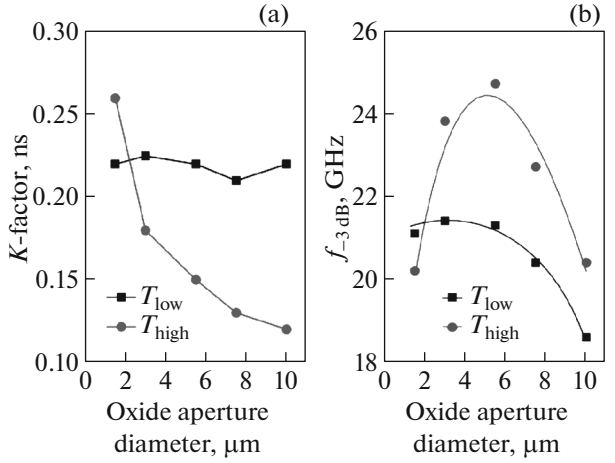

Fig. 9. The dependences of (a) the K factor and (b) modulation bandwidth f_{-3dB} on the size of the current-oxide aperture at the low and high level of losses per the emission output for the VCSEL on the basis of InGaAs QWs with a spectral range of 850 nm. The temperature of measurements is 20°C.

rent due to the high level of damping rate γ of the relaxation oscillations for lasers with relatively small size of current aperture, which indicates the dominance of the mechanism of damping of relaxation oscillations (Fig. 7b). It should be noted that the increase in internal optical losses A_{int}, which are due to the light diffraction at the edges of the oxide aperture [31], and the simultaneous decline of internal quantum efficiency η_i, which is due to the growth of carrier leakage at increased current density [18], are observed when the sizes of the current-oxide aperture are less than 5 μm, which leads to an additional decrease in differential gain of the active region g_N. As a result, the contribution of gain nonlinearity τ_g in the value of the K factor grows at small aperture sizes. In this case, a significant increase in losses in output emission T_m leads to a significant increase in the τ_g component, which compensates the effect of the reduction of lifetime of photons in the cavity τ_p (Fig. 8). In this way, the positive effect of the reduction of the lifetime of the photons in the cavity on the VCSEL modulation bandwidth will be effective only for lasers with an intermediate size of the current aperture (3–7 μm), in which relatively low internal losses remain and the modulation bandwidth is limited by the damping of the relaxation oscillations (Fig. 9). The reduction of the lifetime of photons in the cavity allowed increasing the modulation bandwidth to 24–25 GHz for the VCSEL with a spectral range of 850 nm based on strained InGaAs QWs with the specified dimensions of the current aperture [87].

It should be noted that the increase in the modulation bandwidth due to the reduction of the lifetime of photons in the cavity does not necessarily lead to an increase in the data-transmission rate from the point of view of modulation in a large signal mode (for example, during impulse modulation) [88]. On the one hand, the increase in the K factor leads to growth of the signal-rise time and a decreasing in the optical0signal amplitude, which affects the eye-diagram quality negatively. On the other hand, the decrease in the K factor leads to increased jitter (so-called "timing jitter") and an increase in the signal amplitude overshoot over the logic level "1" (overshoot) in the eye diagram, which limits the digital data error-free trans-

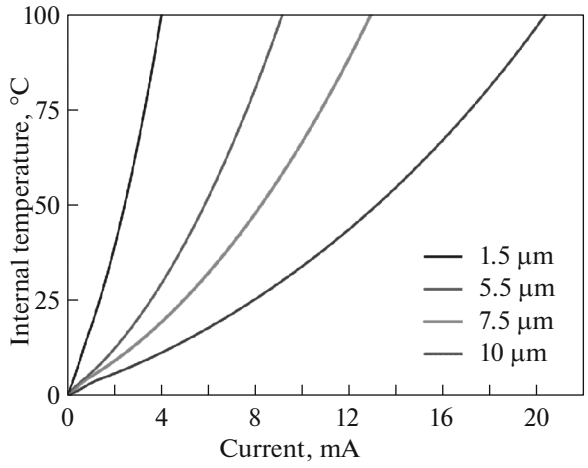

Fig. 10. The dependences of the internal temperature on the pumping current for the VCSEL on the basis of InGaAs QWs with a spectral range of 850 nm with different sizes of the oxide-current aperture. The temperature of measurements is 20°C.

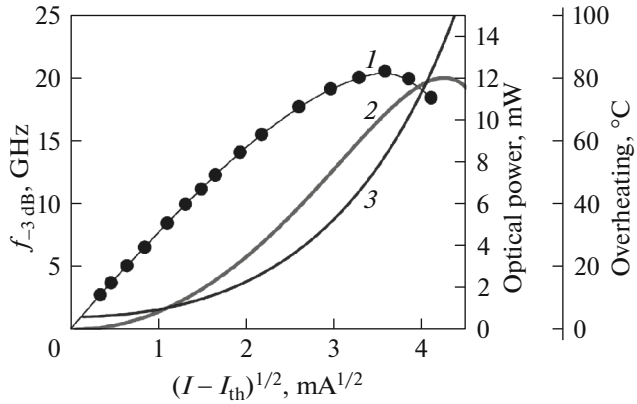

Fig. 11. The dependences of (*1*) modulation bandwidth f_{-3dB}, (*2*) output optical power, and (*3*) the magnitude of the overheating of the active region on $\sqrt{I - I_{th}}$ for the VCSEL on the basis of InGaAs QWs with a spectral range of 850 nm with an oxide-current aperture of 9 μm. The temperature of measurements is 20°C.

mission rate, despite the high modulation bandwidth. Therefore, it is necessary to optimize the value of the damping rate to achieve simultaneously a high modulation bandwidth and low jitter to obtain high-quality eye diagrams (satisfying the standard masks) at the desired data-transmission rate. In [16], it is shown that the error-free data-transmission rate, when the value of the K factor is ~0.17 ns, can be increased up to 57 Gbit/s for a VCSEL with a maximum modulation bandwidth of 23 GHz.

Further increase in the VCSEL high-speed performance is associated with a reduction in heat emission and/or improvement in heat removal, as well as improvement of the electronic and optical constraints.

7. THERMAL EFFECTS

The effect of the internal temperature increasing (the so-called "self-heating effect") for any of the injection lasers leads to a decrease in differential efficiency due to the reduction in the inverse population and an increase in threshold current due to additional optical losses on free carriers, which in turn affects the device high-speed performance negatively. The self-heating effect is pronounced in the VCSEL with an increasing of the pumping current due to the small size of the active region, a large number of heteroboundaries in the path of the charge carriers, and low thermal conductivity of the AlGaAs layers in the DBR. In addition, the VCSEL internal-temperature growth accelerates the degradation of the laser. For example, increasing the active-region temperature from 100 to 150° leads to an increase in the rate of degradation by the order at a typical value of activation energy of ~0.7 eV [89].

In Fig. 10 shows dependences calculated according to [90] of the internal temperature on the pumping current for the VCSEL on the basis of InGaAs QWs with a spectral range of 850 nm with different sizes of the current-oxide aperture. The internal laser temperature depends not only on the pumping current, but also on the current-oxide-aperture size. The thermal resistance of the VCSEL is inversely proportional to the lateral size of the current aperture in the first approximation, whereas the series resistance is inversely proportional to the current-aperture area [18]. As a result, the emitted thermal power is proportional to the current-aperture area at a fixed current density, so the wide-aperture VCSELs have a higher internal temperature at the same current density.

The increased internal temperature causes the saturation of not only the output optical power, but also the resonance frequency (Fig. 11), and the saturation of the resonance frequency occurs at a smaller value of the overheating of the active region than the saturation of the output power. Since the wide-aperture VCSELs overheat more strongly at a given current density, the achievable resonant frequencies for them are significantly lower than for the VCSEL with a small size of the current aperture [74, 87]. At the same time, lasers with a small size of the current aperture exhibit a higher damping rate of the relaxation oscillations (Fig. 7b), which limits their maximum modulation bandwidth.

According to [91], the linear mechanisms of the heat release depending on pumping current, which are related to the leakage currents, thermalization of car-

riers, spontaneous recombination, and internal optical losses, make a significantly greater contribution to the heating of the VCSEL compared to the joule heating on the series resistance of the laser, which depends on the current quadratic. It is necessary not only to reduce the series resistance of the laser, but also to lower the absorption level on free carriers and minimize the thermal resistance of the device design to improve the thermal characteristics of the VCSEL. In addition, it is necessary to suppress the emission of carriers from the active region at an elevated temperature (an additional contribution to the leakage current), which is possible due to the use of heterostructures with a separate restriction of carriers [46] and the introduction of additional potential barriers for electrons (carrier blocking layer) [92].

The method of the decreasing of the *p*-type serial resistance of a DBR by diffusion of zinc can be noted in addition to the basic ways to reduce the VCSEL series resistance that were discussed above. This method allows reducing the differential resistance of the VCSEL with a spectral range of 850 nm by 30% and increasing the modulation bandwidth, first, to 22 GHz for the VCSEL with an current-oxide-aperture size of 4 μm [93] and, then, to 29 GHz for devices with an current-oxide aperture of 3 μm [94].

A further reduction of the internal temperature of the laser is associated with improved heat removal by the reducing the thermal resistance of the VCSEL design, which is primarily determined by the thermal conductivity of the DBR. According to [95], the thermal conductivity of the DBR is anisotropic, the longitudinal component (in the plane of epitaxial layers) is typically twice that of the transverse one, and the presence of graded interfaces in the RBO leads to a further drop in the thermal conductivity in the longitudinal direction. An increase in the thermal conductivity of the DBR Al(Ga)As is possible only when using quarter-wavelength layers based on arsenic binary compounds, which have the greatest thermal-conductivity coefficients. Thus, the use of the DBR AlAs/AlGaAs allows reducing the internal temperature of the VCSEL with a spectral range of 850 nm by 20–30% in comparison with the corresponding value for the RBO based on AlGaAs alternating layers at the same current [86]. A similar approach is also applied to the VCSEL with a spectral range of 980 nm [96]. The elimination of gradient heterointerfaces in mirrors can be used to increase their thermal conductivity, but requires a more complex VCSEL design with intracavity contacts [32, 97].

The most radical solution to the problem of the thermal resistance of the VCSEL is connected to the formation of an additional heat sink from materials with high thermal conductivity. This, the dimensions of a DBR mesa of *p* type can be reduced by 60% while maintaining the required size of the current aperture in the VCSEL design with light output through the substrate, as compared to those for the laser design with light output upward, and the mesa itself can be additionally covered by a thick layer of electroplating gold, which can reduce the thermal resistance of the laser by a factor of 2 and increase the maximum output power by 60%, as well as improve current spreading on the aperture area and reduce the capacitance at the oxide aperture [98]. It should be noted that this idea is applicable only in the region of transparency of the substrate that is used for laser emission. However, this approach was modified for a VCSEL with light output upward: a ring copper layer with a thickness of 2 μm (a so-called "copper heat sink") was deposited on the surface and side walls of the DBR mesa of *p* type, which allowed not only reducing the thermal resistance by 50% and increasing the output power by 130%, but also increasing of the modulation bandwidth by 40% to 10 GHz [99]. However, the parasitic capacitance, which is formed on the thin dielectric layer between the *n* contact and the copper heat sink, contributes to the capacitance of the contact pads and limits the parasitic cutoff frequency of the device, while the topology optimization of the copper heat sink gives only a slight increase in the modulation bandwidth, despite the reduction in parasitic capacitance by a factor of 2.5 [39].

8. ELECTRONIC AND OPTICAL CONFINEMENT

The geometry of an optical microcavity with separate carrier limitation [100] and an optical length of 1–1.5 λ (the geometric distance between the boundaries of the lower and upper DBRs is meant) is widely used to provide effective electronic limitation in the construction of high-speed VCSELs. However, the decrease in the optical length of the microcavities to 0.5λ allows increasing the longitudinal factor of the optical confinement (by 70%) and compensating some growth in losses per emission output, thereby maintaining a high level of the differential gain of the active region [101]. A possible embodiment of the VCSEL on the basis of InGaAs QWs with a spectral range of 850 nm with a 0.5-λ microcavity is presented in Fig. 12. The proposed approach also leads to the reduction of the mode volume and decreasing of the damping rate of the relaxation oscillations, as well as improvement of carrier transport, which allowed the increasing of the modulation bandwidth of the VCSEL with a spectral range of 980 nm by more than 30% (from 14 to 20 GHz) and exhibiting error-free data transmission at the rate of 40 Gbit/s up to 85°C for the VCSEL with an aperture of 6 μm [64, 96]. The further reduction of the dimension of the aperture to 4.5–5 μm and decrease in the lifetime of photons in the microcavity by increasing the thickness of the near-surface layer of the DBR led to the increasing of

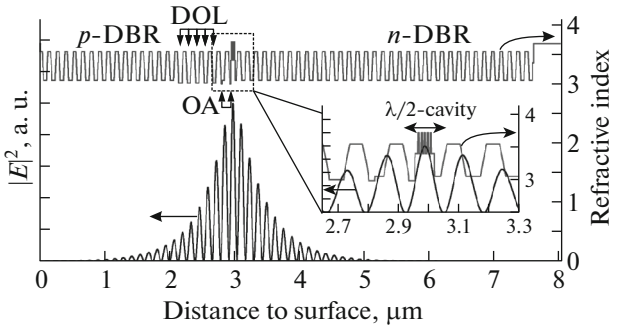

Fig. 12. The calculated electromagnetic-field distribution of the standing wave and the profile of the refractive index in the VCSEL on the basis of InGaAs QWs with a spectral range of 850 nm with a 0.5-λ microcavity and an asymmetrical arrangement of the aperture layers. The inset shows an enlarged image of the optical-microcavity design. The designations are the same as in Fig. 2.

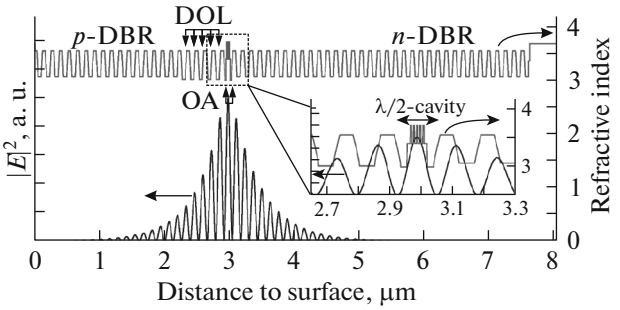

Fig. 13. The calculated electromagnetic-field distribution of the standing wave and the profile of the refractive index in the VCSEL on the basis of InGaAs QWs with a spectral range of 850 nm with a 0.5-λ microcavity and a symmetrical arrangement of the aperture layers. The inset shows an enlarged image of the optical-microcavity design. The designations are the same as in Fig. 2.

the modulation bandwidth to 24.7 GHz and implementation of the error-free data transmission at the rate of 50 Gbit/s [102]. It should be noted that the location of the current-oxide aperture in the microcavity relative to the active region also has an impact on the VCSEL modulation bandwidth. According to [15], the decrease in the internal quantum efficiency (to 65–70%) due to the lateral spreading of carriers under the aperture is observed in the case of the location of the current-oxide aperture in the second and third pairs of the DBR relatively active region that compensates the positive effect of the growth of the longitudinal factor of the optical confineement (by 20%). However, the decrease of the transport coefficient due to the drop of the time of charge-carrier transfer through the *i* region in the 0.5 λ microcavity along with a low *K* factor (0.15–0.16 ns) allowed increasing the modulation bandwidth of the VCSEL with a spectral range of 850 nm to 27–28 GHz and achieve an error-free data-transmission rate of 47 Gbit/s [15, 103].

The application of the design of a 0.5-λ microcavity, which was symmetrically constrained by oxide layers, was the logical continuation of this approach, which led not only to an increase in the longitudinal factor of the optical confinement, but also to an improvement of the transverse factor of the optical confinement (especially at small sizes of the current aperture), as well as increasing of the internal quantum efficiency (up to 81–86%) [104]. A possible variant of a VCSEL based on InGaAs QWs with a spectral range of 850 nm and a 0.5-λ microcavity and symmetrical arrangement of the aperture layers is presented in Fig. 13. The reduction of the size of the current aperture to 3.5 μm and minimization of the *K* factor (~0.13 ns) allowed the increasing of the modulation bandwidth of the VCSEL to a record value of 30 GHz in the mode of direct-current modulation [77].

At the same time, it is shown in [52] that a strong optical confinement in a short microcavity can lead to earlier saturation of the output optical power. At the same time, the time of the hole transport through the *i* region is significantly higher than the time of the electron transfer due to the higher effective mass in a long microcavity, which leads to growth of the transport coefficient and a decrease in the modulation bandwidth. However, the use of the asymmetric microcavity design with an optical length of 1.5 λ, in which the active region is moved closer to layers of *p* type, allows reaching a compromise between the output power and modulation bandwidth. This approach increased the modulation bandwidth of a single-mode VCSELs from 11 to 14 GHz and the saturation current of the optical power from 8 to 10 mA.

The reduction of the penetration depth of the optical mode in distributed Bragg reflectors by applying the design of a VCSEL with intracavity contacts and an output dielectric mirror with a high refractive-index contrast is an alternative way to increase the optical confinement factor [97]. However, this method is most effective from the point of view of increasing the efficiency of a laser, but the maximum error-free transmission rate for a VCSEL with a spectral range of 1060 nm in this design does not exceed 25 Gbit/s [105].

9. CONCLUSION

It follows from the presented review that the proposed methods for providing high-speed performance of the VCSEL of the near-infrared range in the mode of direct-current modulation can raise the modulation bandwidth up to 30 GHz and increase the data-transmission rate up to 55–57 Gbit/s at an amplitude modulation on the NRZ code. It appears that a significant

improvement in the dynamic characteristics of the VCSEL of near-infrared range in the mode of direct-current modulation is very problematic. The use of special schemes for optical-signal-form equalization on both the transmitter and receiver allowed achieving a record-high data-transmission rate of 71 Gbit/s [106]. The further increase in the data-transmission rate along an optical channel is associated with the use of multilevel modulation formats such as pulse-amplitude modulation, discrete multitone modulation, and carrierless amplitude/phase modulation [107]. It should be noted that the data-modulation methods require the use of more complex electronic circuits with higher power consumption, despite the possibility of using VCSEL direct-current modulation in the transmitter and the use of the well-developed $p-i-n$ photodetectors in the receiver in these approaches.

REFERENCES

1. *VCSELs: Fundamentals, Technology and Applications of Vertical-Cavity Surface Emitting Lasers*, Ed. by R. Michalzik (Springer, Berlin, 2013).
2. H. Soda, K. Iga, C. Kitahara, et al., Jpn. J. Appl. Phys. **18**, 2329 (1979).
3. J. K. Guenter, R. A. Hawthorne, D. N. Granville, et al., Proc. SPIE **2683**, 102 (1996).
4. D. M. Kuchta, P. Pepeljugoski, and Y. Kwark, in *Proceedings of the LEOS Summer Topical Meeting* (IEEE, 2001), p. 49.
5. N. Suzuki, H. Hatakeyama, K. Fukatsu, et al., in *Proceedings of the Optical Fiber Communications Conference, Anaheim, USA, 2006*, p. OFA4.
6. K. Yashiki, N. Suzuki, K. Fukatsu, et al., in *Proceedings of the Optical Fiber Communications Conference, Anaheim, USA, 2007*, p. OMKI.
7. Y.-C. Chang, C. S. Wang, and L. A. Coldren, Electron. Lett. **43**, 1022 (2007).
8. T. Anan, N. Suzuki, K. Yashiki, et al., in *Proceedings of the International Symposium on VCSELs and Integrated Photonics, Tokyo, Japan, 2007*, p. E3.
9. P. Westbergh, J. S. Gustavsson, A. Haglund, et al., Electron. Lett. **44**, 907 (2008).
10. R. Johnson and D. Kuchta, in *Proceedings of the Conference on Lasers and Electro-Optics, San Jose, USA, 2008*, p. CMW2.
11. P. Westbergh, J. S. Gustavsson, A. Haglund, et al., Electron. Lett. **45**, 366 (2009).
12. S. A. Blokhin, J. A. Lott, A. Mutig, et al., Electron. Lett. **45**, 501 (2009).
13. P. Westbergh, J. S. Gustavsson, B. Kügel, et al., Proc. SPIE **7952**, 79520K (2011).
14. W. Hofmann, P. Moser, P. Wolf, et al., in *Proceedings of the Optical Fiber Communications Conference, Los Angeles, USA, 2011*, p. PDPC5.
15. P. Westbergh, R. Safaisini, E. Haglund, et al., IEEE Photon. Technol. Lett. **25**, 768 (2013).
16. P. Westbergh, E. P. Haglund, E. Haglund, et al., Electron. Lett. **49**, 1021 (2013).
17. R. S. Tucker, IEEE J. Lightwave Technol. **3**, 1180 (1985).
18. L. A. Coldren and S. W. Corzine, *Diode Lasers and Photonic Integrated Circuits* (Wiley, New York, 1995).
19. G. P. Agraval, *Fiber Optic Communication Systems* (Wiley, New York, 1997).
20. A. K. Dutta, H. Kosaka, K. Kurihara, et al., IEEE J. Lightwave Technol. **16**, 870 (1998).
21. K. Y. Lau and A. Yariv, IEEE J. Quantum Electron. **21**, 121 (1985).
22. A. N. Al-Omari and K. L. Lear, IEEE Photon. Technol. Lett. **16**, 969 (2004).
23. A. N. Al-Omari and K. L. Lear, IEEE Trans. Dielectr. Electr. Insul. **12**, 1151 (2005).
24. K. Kojima, R. A. Morgan, T. Mullally, et al., Electron. Lett. **29**, 1771 (1993).
25. G. Reiner, E. Zeeb, B. Möller, et al., IEEE Photon. Technol. Lett. **7**, 730 (1995).
26. E. F. Schubert, L. W. Tu, G. J. Zydzik, et al., Appl. Phys. Lett. **60**, 466 (1992).
27. K. L. Lear and R. P. Schneider, Appl. Phys. Lett. **68** (5), 29 (1996).
28. M. G. Peters, B. J. Thibeault, D. B. Young, et al., Appl. Phys. Lett. **63**, 3411 (1993).
29. P. G. Newman, J. Pamulapati, H. Shen, et al., J. Vac. Sci. Technol. B **18**, 1619 (2000).
30. J. Strologas and K. Hess, IEEE Trans. Electron Dev. **51**, 506 (2004).
31. E. R. Hegblom, D. I. Babic, B. J. Thibeault, et al., Appl. Phys. Lett. **68**, 1757 (1996).
32. Y.-C. Chang and L. A. Coldren, IEEE J. Sel. Top. Quantum Electron. **15**, 704 (2009).
33. A. M. Nadtochiy, S. A. Blokhin, A. G. Kuz'menkov, M. V. Maksimov, N. A. Maleev, S. I. Troshkov, N. N. Ledentsov, V. M. Ustinov, A. Mutig, and D. Bimberg, Tech. Phys. Lett. **38**, 106 (2012).
34. B. M. Hawkins, R. A. Hawthorne III, J. K. Guenter, et al., in *Proceedings of the 52nd IEEE Electronic Components and Technology Conference* (IEEE, 2002), p. 540.
35. M. Azuchi, N. Jikutani, M. Arai, et al., in *Proceedings of the Conference on Lasers and Electro-Optics* (USA, Baltimore, 2003), Vol. 1, p. 163.
36. Y. Ou, J. S. Gustavsson, P. Westbergh, et al., IEEE Photon. Technol. Lett. **21**, 1840 (2009).
37. A. Larsson, P. Westbergh, J. Gustavsson, et al., Semicond. Sci. Technol. **26**, 014017 (2011).
38. K. L. Lear, V. M. Hietala, H. Q. Hou, et al., OSA Trends Opt. Photonics Ser. **15**, 69 (1997).
39. K. L. Lear and A. N. Al-Omari, Proc. SPIE **6484**, 64840J (2007).
40. S. W. Corzine, R. H. Yan, and L. A. Coldren, Appl. Phys. Lett. **57**, 2835 (1990).
41. I. Suemune, IEEE J. Quantum Electron. **27**, 1149 (1991).
42. L. F. Lester, S. D. Offsey, B. K. Ridley, et al., Appl. Phys. Lett. **59**, 1162 (1991).

43. J. D. Ralston, S. Weisser, I. Esquivias, et al., IEEE J. Quantum Electron. **29**, 1648 (1993).
44. A. Mutig, J. A. Lott, S. A. Blokhin, et al., Appl. Phys. Lett. **97**, 151101 (2010).
45. S. B. Healy, IEEE J. Quantum Electron. **46**, 504 (2010).
46. P. Westbergh and J. Gustavsson, IEEE J. Sel. Top. Quantum Electron. **15**, 694 (2009).
47. Y. Arakawa and A. Yariv, IEEE J. Quantum Electron. **22**, 1887 (1986).
48. K. Uomi, Jpn. J. Appl. Phys. **29**, 81 (1990).
49. K. Uomi, T. Mishima, and N. Chinone, Jpn. J. Appl. Phys. **29**, 88 (1990).
50. T. Takahashi, M. Nishioka, and Y. Arakawa, Appl. Phys. Lett. **58**, 4 (1991).
51. Y. Zheng, C.-H. Lin, A. V. Barve, et al., in *Proceedings of the IEEE Photonics Conference IPC 2012, Burlingame, CA, Sept. 23–27, 2012* (IEEE, 2012), p. 131.
52. K.-L. Chi, D.-H. Hsieh, J.-L. Yen, et al., IEEE J. Quantum Electron. **52**, 2400607 (2016).
53. M. Grundmann and D. Bimberg, Phys. Status Solidi A **164**, 297 (1997).
54. A. E. Zhukov, M. V. Maksimov, and A. R. Kovsh, Semiconductors **46**, 1225 (2012).
55. N. N. Ledentsov, V. M. Ustinov, V. A. Shchukin, et al., Semiconductors **32**, 343 (1998).
56. H. Su and L. F. Lester, J. Phys. D: Appl. Phys. **38**, 2112 (2005).
57. C. Z. Tong, D. W. Xu, S. F. Yoon, et al., in *Proceedings of the 2nd IEEE International Conference on Broadband Network and Multimedia Technology IC-BNMT'09* (IEEE, 2009), p. 906.
58. D. W. Xu, S. F. Yoon, Y. Ding, et al., IEEE Photon. Technol. Lett. **23**, 91 (2011).
59. Y. Ding, W. J. Fan, D. W. Xu, et al., J. Phys. D: Appl. Phys. **42**, 085117 (2009).
60. H. Dery and G. Eisenstein, IEEE J. Quantum Electron. **41**, 26 (2005).
61. D. R. Matthews, H. D. Summers, P. M. Smowton, et al., Appl. Phys. Lett. **81**, 4904 (2002).
62. M. V. Belousov, N. N. Ledentsov, M. V. Maximov, et al., Phys. Rev. B **51**, 14346 (1995).
63. A. Mutig, G. Fiol, P. Moser, et al., Electron. Lett. **44**, 1345 (2008).
64. A. Mutig, J. A. Lott, S. A. Blokhin, et al., IEEE J. Sel. Top. Quantum Electron. **17**, 1568 (2011).
65. A. M. Nadtochiy, S. A. Blokhin, A. Mutig, J. A. Lott, N. N. Ledentsov, L. Ya. Karachinskiy, M. V. Maximov, V. M. Ustinov, and D. Bimber, Semiconductors **45**, 679 (2011).
66. P. Wolf, P. Moser, G. Larisch, et al., IEEE J. Sel. Top. Quantum Electron. **19**, 1701207 (2013).
67. J. Tatum, in *Proceedings of the Symposium on Broadband Communications for the Internet Era* (IEEE, 2001), p. 58.
68. A. Mutig, G. Fiol, K. Pötschke, et al., IEEE J. Sel. Top. Quantum Electron. **15**, 679 (2009).
69. M. S. Torre and H. F. Ranea-Sandoval, IEEE J. Quantum Electron. **36**, 112 (2000).
70. S. A. Blokhin, M. A. Bobrov, N. A. Maleev, et al., Appl. Phys. Lett. **105**, 061104 (2014).
71. S. A. Blokhin, J. A. Lott, N. N. Ledentsov, et al., Proc. SPIE **8308**, 830819 (2011).
72. A. Mutig, J. A. Lott, S. A. Blokhin, et al., Proc. SPIE **7952**, 79520H (2011).
73. L. Ya. Karachinsky, S. A. Blokhin, I. I. Novikov, et al., Semicond. Sci. Technol. **28**, 065010 (2013).
74. J. A. Lott, A. S. Payusov, S. A. Blokhin, et al., Phys. Status Solidi C **9**, 290 (2012).
75. P. Moser, J. A. Lott, and D. Bimberg, IEEE J. Sel. Top. Quantum Electron. **19**, 1702212 (2013).
76. H. Li, P. Wolf, P. Moser, et al., IEEE J. Sel. Top. Quantum Electron. **21**, 1700409 (2015).
77. E. Haglund, P. Westbergh, J. S. Gustavsson, et al., Electron. Lett. **51**, 1096 (2015).
78. J.-W. Shi, C.-C. Chen, Y.-S. Wu, et al., IEEE J. Quantum Electron. **45**, 800 (2009).
79. M. P. Tan, S. T. M. Fryslie, J. A. Lott, et al., IEEE Photon. Technol. Lett. **25**, 1823 (2013).
80. M. Tan, A. M. Kasten, J. D. Sulkin, et al., IEEE J. Sel. Top. Quantum Electron. **19**, 4900107 (2013).
81. Å. Handlung, J. S. Gustavsson, J. Vukusic, et al., IEEE Photon. Technol. Lett. **16**, 368 (2004).
82. J. S. Gustavsson, Å. Handlung, J. Bengtsson, et al., IEEE J. Quantum Electron. **40**, 607 (2004).
83. R. Safaisini, E. Haglund, P. Westbergh, et al., Electron. Lett. **50**, 40 (2014).
84. E. Haglund, Å. Haglund, P. Westbergh, et al., Electron. Lett. **48**, 517 (2012).
85. P. Westbergh, J. S. Gustavsson, B. Kögel, et al., Electron. Lett. **46**, 938 (2010).
86. P. Westbergh, J. S. Gustavsson, B. Kögel, et al., IEEE J. Sel. Top. Quantum Electron. **17**, 1603 (2011).
87. M. A. Bobrov, S. A. Blokhin, A. G. Kuzmenkov, N. A. Maleev, A. A. Blokhin, Yu. M. Zadiranov, E. V. Nikitina, and V. M. Ustinov, Semiconductors **48**, 1657 (2014).
88. E. P. Haglund, P. Westbergh, J. S. Gustavsson, et al., IEEE J. Lightwave Technol. **33**, 795 (2015).
89. J. Wang, C. Ji, D. Soderstrom, T. Jian, et al., Proc. SPIE **7952**, 795205 (2011).
90. M. Osinski and W. Nakwaski, Int. J. High Speed Electron. Syst. **5**, 667 (1994).
91. P. P. Baveja, B. Kögel, P. Westbergh, et al., Opt. Express **19**, 15490 (2011).
92. Y.-A. Chang, T.-S. Ko, J.-R. Chen, et al., Semicond. Sci. Technol. **21**, 1488 (2006).
93. J.-W. Shi, J.-C. Yan, J.-M. Wun, et al., IEEE J. Sel. Top. Quantum Electron. **19**, 7900208 (2013).
94. J.-W. Shi, C.-C. Wei, J. Chen, et al., Proc. SPIE **10122**, 101220F (2017).
95. J. Piprek, T. Tröger, B. Schröter, et al., IEEE Photon. Technol. Lett. **10**, 81 (1998).
96. P. Moser, P. Wolf, A. Mutig, et al., Appl. Phys. Lett. **100**, 081103 (2012).

97. K. Takaki, S. Imai, S. Kamiya, et al., Proc. SPIE **7952**, 795204 (2011).

98. T. Wipiejewski, D. B. Young, M. G. Peters, et al., Electron. Lett. **31**, 279 (1995).

99. A. N. Al-Omari, G. P. Carey, S. Hallstein, et al., IEEE Photon. Technol. Lett. **18**, 1225 (2006).

100. Y. Liu, W.-C. Ng, F. Oyafuso, et al., IEE Proc. Optoelectron. **149**, 182 (2002).

101. A. Mutig and D. Bimberg, Adv. Opt. Technol. **2011**, 290508 (2011).

102. P. Moser, J. A. Lott, P. Wolf, et al., Electron. Lett. **50**, 1369 (2014).

103. P. Westbergh, R. Safaisini, E. Haglund, et al., Electron. Lett. **48**, 1145 (2012).

104. E. Haglund, P. Westbergh, J. S. Gustavsson, et al., IEEE J. Lightwave Technol. **34**, 269 (2016).

105. A. Kasukawa and Y. Kawakita, in *Proceedings of the IEEE Photonics Conference IPC 2015, Reston, Virginia, Oct. 4–8, 2015* (IEEE, 2015), p. 585.

106. D. M. Kuchta, A. V. Rylyakov, F. E. Doany, et al., IEEE Photon. Technol. Lett. **27**, 577 (2015).

107. N. N. Ledentsov, N. Ledentsov, Jr., M. Agustin, et al., Nanophotonics **6**, 813 (2017).

Translated by N. Petrov